

Experimental evidence of MCSA for the diagnosis of ball-bearings

Fabio IMMOVILLI¹, Marco LIPPI², Marco COCCONCELLI³

DISMI, University of Modena and Reggio Emilia, 42123 Reggio Emilia, Italy
{¹fabio.immovilli,²marco.lippi,³marco.cocconcelli}@unimore.it

Abstract

Electrical and mechanical fault diagnosis in induction machines is an extensively investigated field for cost and maintenance savings, as induction motors operating at mains frequency are still the most widespread rotating electric machines employed in industry. Many papers can be found in the literature concerning the general condition monitoring of induction machines. Bearing faults are one of the most common failures in electrical machines: bearing faults that are not detected in time cause malfunction, reduced efficiency, and may even lead to failure of the driven machinery. Online fault detection can be obtained by vibration analysis, but the diagnosis equipment is costly and invasive, requiring dedicated equipment and specific sensors to be installed. Motor current signature analysis (MCSA) is an alternative method that relies on the monitoring of electrical quantities, that are already acquired in the final application, e.g., to implement the control of an electric drive, thus do not require the installation of dedicated transducers. Many research activities were focused on the diagnosis of bearing faults by MCSA. The use of suitable signal processing techniques is required to efficiently extract the fault signatures from raw signals. The use of current and/or voltage signal constitutes a noninvasive method to bring information necessary to diagnose a fault in the system via online monitoring of the electric machine. This paper details the results of a laboratory trial comprising different test sets on the condition monitoring and fault diagnostic of a six-poles induction motor, using a design of experiment (DOE) approach. The manuscript summarizes the results of research that the authors did in the last years, and the aim of the paper is giving a unified point of view on the work done. After the selection of a proper fault-related scalar value, the DOE proves its robustness against setup and working conditions of the motor. Finally, the same scalar value will be proved to be effective as input to long short-memory networks, for automatic condition monitoring of faulted bearings.

1 Introduction

Electrical and mechanical fault diagnosis in induction machines is an extensively investigated field for cost and maintenance savings, as induction motors operating at mains frequency are still the most widespread rotating electric machines in industry, mainly because of their low price, ruggedness and reliability.

Many papers can be found in the literature concerning the general condition monitoring of induction machines [1], [2]. The distribution of failures within the machine sub-assemblies is reported in many reliability survey papers [3]. A rough classification identifies four classes: bearings faults, stator related faults, rotor related faults, other faults (lack of cooling, loose terminal box connection). Bearing faults are one of the most common failures in electrical machines especially in the small-medium power sizes [4]. Bearing faults that are not detected in time cause malfunction, loss of performance, reduced efficiency and may even lead to failure of the driven machinery, [5].

In many situations diagnostics methods based on the analysis of the vibration signals have proved their effectiveness [6], [7]. Among the mechanical problems detected by vibration spectra there are: imbalance, misalignment, loose fitting, bent shafts, and bearing localized faults. On-line fault detection can be obtained by vibration analysis, but the diagnosis equipment is costly and invasive, requiring dedicated equipment and specific sensors to be installed.

Motor current signature analysis (MCSA) is an alternative method that relies on the monitoring of electrical quantities, that are already acquired in the final application, e.g. to implement the control of an electric

drive, thus do not require the installation of dedicated transducers. Many research activities were focused on the diagnosis of bearing faults by MCSA [8]. In many cases mechanical signals cannot be directly acquired, e.g. in harsh environments, remote locations, or because the application is difficult to access. Under such conditions, electric signal measurements would be preferable as they are more immune to external disturbances, [9]. Non-invasive fault diagnosis should ideally detect faults at the early stage, to allow for scheduled maintenance, minimizing system downtime. Under these circumstances, fault signature components feature a very small amplitude that is usually buried in noise and can lead to false positive detection [10]. The use of suitable signal processing techniques is required to efficiently extract the fault signatures from raw signals. The use of current and/or voltage signal constitutes a non-invasive method to bring information necessary to diagnose a fault in the system via on-line monitoring of the electric machine.

Thanks to a dedicated test bench, a laboratory trial comprising different test sets on the condition monitoring and fault diagnostic of a 6-poles induction motor using a design of experiment (DOE) approach was performed. Four different data were acquired (namely vibration data, currents, motor torque and radial force on the motor shaft) and post-processed. This paper focuses on the results of the MCSA, while the analysis of the vibration data is given only as comparison if a reference is needed. The diagnostic techniques used are three: a spectral analysis with an ad-hoc pre-processing, the DOE analysis to qualify the effects of the setup parameters and a machine learning approach based on Long Short-Term Memory (LSTM), particularly suited for the analysis and classification of time-series.

The paper is organized as follows: section 2 reviews the relationship between vibration and current components presented in literature. Section 3 presents the experimental setup with a description on the test bench. Section 4 outlines the two methodologies adopted, specifically the factorial design of experiment and the machine learning technique. The results for test runs under different working conditions and bearing damage are reported in section 5, followed by Conclusion.

2 Currents Based Condition Monitoring

Numerous papers in literature deal with the detection and diagnosis of electro-mechanical faults based on MCSA in induction motors. The link between vibrations and motor current spectral components is still under investigation in the scientific community and is treated in literature according to different approaches.

In the first one, the vibration component causes a rotor eccentricity [14].

The second one links the vibration component to a torque ripple that produces a speed ripple on the electric machine [13]. A unifying approach is presented in [15]. Mechanical vibrations result in a torque ripple that generates in the current a chain of components at frequencies F_{be} :

$$F_{be} = | f \pm k f_{car} | \quad (1)$$

where k is an integer.

Radial bearings consist of two concentric rings containing inner and outer races, separated by rolling elements, Fig. 1. Rolling elements are separated by a cage: a component that maintains a constant angular pitch between adjacent rolling elements, preventing contacts.

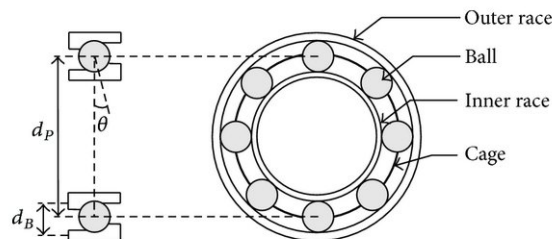


Figure 1: Bearing structure and characteristic dimensions.

Localized faults will produce characteristic vibration frequency components. These bearing fault frequencies are a function of the bearing geometry and the relative speed of the outer and the inner ring. Characteristic

vibration frequencies can be calculated from the bearing's physical dimensions, Fig. 1. In particular, considering the outer ring fixed to the frame:

$$F_{cage} = \frac{1}{2} F_r \left(1 - \frac{D_b \cos \theta}{D_p} \right) \quad (2)$$

$$F_{outer} = \frac{Z}{2} F_r \left(1 - \frac{D_b \cos \theta}{D_p} \right) \quad (3)$$

$$F_{inner} = \frac{Z}{2} F_r \left(1 + \frac{D_b \cos \theta}{D_p} \right) \quad (4)$$

$$F_{ball} = \frac{D_p}{D_b} F_r \left[1 - \left(\frac{D_b \cos \theta}{D_p} \right)^2 \right] \quad (5)$$

where D_b stands for the ball diameter, D_p for the pitch diameter, Z for the number of rolling elements, θ for the ball contact angle, Fig.1. Table 1 summarizes the corresponding vibration related components on the machine current for the torque fluctuation model.

	Model based on torque fluctuations
Outer raceway defect	$f \pm k F_{outer}$
Inner raceway defect	$f \pm k F_{inner}$
Ball defect	$f \pm k F_{ball}$
Cage defect	$f \pm k F_{cage}$

Table 1: Vibration related components in the stator current spectrum.

Considering the torque ripple model, vibration effects on machine currents are caused by small speed fluctuations of the rotor. Because of electromechanical filtering effects (due to the rotor inertia and winding inductance) MCSA is in general more sensitive to low frequency phenomena.

To sum it up, it is usually very difficult to retrieve bearing fault signature components by MCSA. Especially because when dealing with realistic incipient faults, the fault signature is buried in noise or it is only a small fraction of the fundamental supply current component, especially when operating at rated load. In [16] the torque ripple associated with a realistic (not drilled) localized fault was experimentally measured: the peak value of the torque ripple was 3-4 orders of magnitude smaller than the nominal torque of the machine.

3 Test setup

The experimental setup, Fig. 2, comprises the electrical motor under test (MUT) that is installed on a test bench in order to vary both the radial and the torque load conditions. The chosen MUT is a three phase induction machine operated directly connected to the 50 Hz mains grid. The test bench also houses a brake/dynamometer consisting of a vector controlled induction machine in order to vary the load torque on the MUT. Table 2 summarizes the nameplate data of the MUT.

Nominal Power	1100	[W]
Number of poles	6	
Nominal current	2.8	[A]
Power Factor	0.76	
Nominal Torque	11.5	[Nm]
Stator Resistance	5.65	[Ω]

Table 2: Nameplate data of the Motor Under Test

Radial load on the MUT shaft is provided by a specially designed test fixture, comprising a pneumatic cylinder coupled to a manifold with pressure regulator and transducer to modulate the radial load. The cylinder is connected to a crosshead carrying an extension shaft that allows to apply a variable radial force at the motor

Table 3: Specifications of the ball bearing and expected fault frequencies

Supply frequency (f)	50 [Hz]	F_r	15.9 [Hz]
Inner diameter	25 [mm]	F_{inner}/F_r	5.41
Outer diameter	52 [mm]	F_{outer}/F_r	3.585
Number of spheres	9	F_{cage}/F_r	0.398
Basic static load rating	7800 [N]	F_{ball}/F_r	4.715

shaft's end. The cylinder is supplied with compressed air at a pressure up to 6 bar, corresponding to a radial force of up to 1180 N exerted on the front bearing.

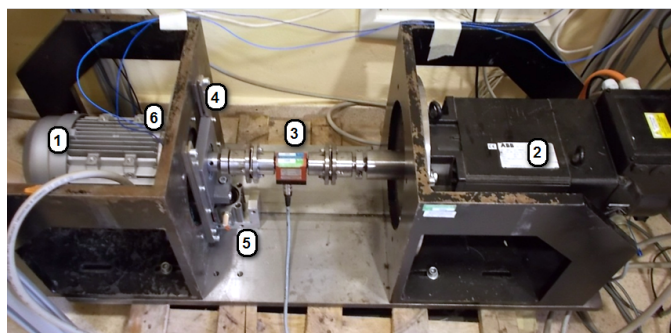


Figure 2: Test setup overview: (1) MUT; (2) brake/dynamometer; (3) torque meter; (4) crosshead; (5) pneumatic cylinder; (6) accelerometer position. The compressed air hose connecting the cylinder to the manifold with pressure regulator and transducer is not shown.

The test bearing is a SKF 6205 deep groove ball bearing. Table 3 summarizes the characteristic fault frequencies with the MUT operated at nominal frequency.

Two different damages were artificially made on the bearings, in order to apply DOE to different data test set: A single defect on the outer raceway, created by chemical etching of the bearing outer race, Fig. 3-left. A simulated brinelling defect, generated applying a mechanical load of 4 tons (40 kN) to the bearing, Fig. 3-right.



Figure 3: Micrograph of the chemically etched outer race defect (left). Photo of the hydraulic press employed to impart bearing brinelling damage (right).

The physical quantities monitored are: the radial vibration of the motor, the stator currents fed to the machine, the radial force exerted by the pneumatic cylinder and the load torque at the motor shaft. The vibration of the motor is measured by means of a mono-axial accelerometer placed on the frame of the test rig (sensitivity: 10.28 mV/g). The currents are measured by means of LEM LTSR 6-NP closed loop Hall current transducers (nominal current: 6 Arms; output voltage: 104,16 mV/A, accuracy: $\pm 0,2\%$) and the pressure by mean of a pressure sensor (output voltage: 0–10 V; measurement range: 0–10 bar, accuracy: $\pm 0,5\%$). The torque is measured by a torque meter mounted between the motor and the brake shafts (maximum torque: 20 Nm, linearity: $\pm 0,2\%$ of full scale).

4 Methods

4.1 Design of experiment

The Design of Experiment (DOE) procedure, a powerful statistical technique based on the analysis of variance (ANOVA), can be conveniently applied to multivariable problems. The DOE is the branch of science that deals with designing the correct sequence of experiments to minimize measurement errors and maximize the evidence of dependencies between causes and results [12].

The inputs to the system are called “factors” and each of them could have more than one value (usually called “levels”). The number of factors and the number of levels determine the complexity of the experimental plan and the total number of tests to be done. The DOE approach fixes some procedures in order to minimize the influence of parameters other than the selected inputs, and proposes statistical tools to determine the significance of dependencies between the input and output of the system [17].

In this paper, the design of experiment for each test set consists of three independent factors with two levels each: the value of radial load, the load torque and the type of damage on the front bearing. Table 4 summarizes the factors and levels used in the first and second test run.

First test set			
Factors:	Radial load	Load torque	Bearing status
Level 1	3 bar / 590 N	50%	healthy
Level 2	6 bar / 1180 N	100%	Outer race
Second test set			
Factors:	Radial load	Load torque	Bearing status
Level 1	3 bar / 590 N	50%	healthy
Level 2	6 bar / 1180 N	100%	Brinelling

Table 4: Factors and levels of the independent variables used in the Design Of Experiment (DOE).

Two test set were performed in the laboratory trial, one employing a bearing with a localized fault on the outer race, the other employing a bearing with artificial brinelling. The resulting full factorial experimental plans consist of 8 randomized tests each, which are not replicated. The statistical analysis software Minitab was used to lay out the randomized test plan and to perform the analysis of variance (ANOVA) on the results. The levels of the independent variables were normalized: torque was normalized to the rated torque of the machine, radial load was normalized to the maximum value obtainable, while the fault is modeled as a binary variable (healthy = 0, faulty = 1).

The current signal has been filtered by a series of notch filters in order to the remove the 50 Hz fundamental mains supply frequency and its higher harmonics over all the frequency range. The Root Mean Square (RMS) value of the filtered current is taken as response factor for the ANOVA analysis. The RMS is used to take into account the energy of the residual signal, considering that any damage to the motor requires additional energy, appearing in the spectrum as sideband modulations according to Table 1. Since the torque ripple due to the bearing fault impacts is independent of the torque load on the machine, the residual signal was chosen as a good candidate for a robust scalar fault index.

Figure 4 shows the post-processing flowchart of the current signal, where X is the input current signal, Y is the residual signal after the filtering and Z is the RMS value.



Figure 4: Flowchart of the current signal processing.

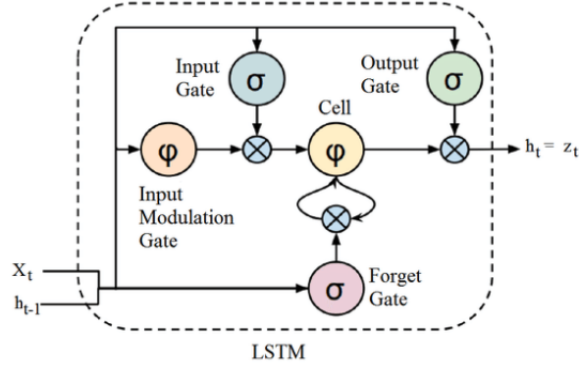


Figure 5: Depiction of LSTM cell. σ (input, output, forget gates) are typically the sigmoid function. Recurrent connections h_t and X_t propagate information through time.

4.2 Long Short-Term Memory Networks

Long Short-Term Memory Networks (LSTMs) are a class of recurrent neural networks. They are designed specifically to process periodic input sequences, such as time-series. They were first introduced in the late nineties [11], and demonstrated high performance in different tasks pertaining pattern recognition and sequence classification. Only during the last decade and thanks to the largely increased interest in neural networks, LSTMs became the state-of-the-art in different application domains pertaining both to the industry and the research [20]). Recurrent networks are capable of processing time sequences of arbitrary length. The output of a RNN is not simply a function of the actual input, but it is also function of the internal *state* of the network. The output of a generic cell h_t^ℓ in layer ℓ at time t is a function of both the input of that layer (x_t) and of the previous output of the same cell at the time step (h_{t-1}^ℓ). During training, classic RNNs suffer from a problem named “vanishing gradient” [21]. That limitation greatly hinders their applicability in many practical classification tasks. LSTMs were introduced to the particular aim of overcoming this limitation, thanks to the implementation of a *memory cell* with a more complex structure. In simple terms, LSTM cells can maintain their state over time, or forget what they have learned and also to allow new information in. In order to overcome overfitting issues, LSTMs make use of a form of regularization called dropout [22]: during the training phase the inter-layer connections between cells are randomly dropped with probability $(1 - p)$ and, at prediction time, all the weights are multiplied by p .

Figure 5 illustrates the schematic structure of such a cell. The cell’s status X_t depends on three non-linear gates that control the information flow: the input gate, which allows new information to enter the state; the forget gate, that controls how much of the value contained in the previous state is kept or forgotten at a given time and the output gate that transfers the information to the upper layers.

The network input data, in the present work, is the time-series of the three phase current signals, pre-processed to obtain the residual signal (Y signal in Fig.4). More specifically, each example fed to the network is a $3 \times W$ matrix, where W is a preset window length of samples of each of the current signals.

5 Results

5.1 DOE results

The test runs were performed according to the DOE and the physical quantities defined in Section 4.1 were acquired using 24 Bit, 51.2 kS/s data acquisition modules: for each test run, a 10 s length file was recorded for post processing and analysis.

Figure 6 shows - on the same picture - a comparison of the spectrum of the current signal, in case of healthy and faulty front bearing (localized defect on the outer race). For uniformity of presentation, both the faulty and the healthy case shown are for a machine operated at rated output torque and 6 bar pressure on the radial load cylinder. The sidebands already present are due to the intrinsic unbalance of the electric machine caused by manufacturing tolerances.

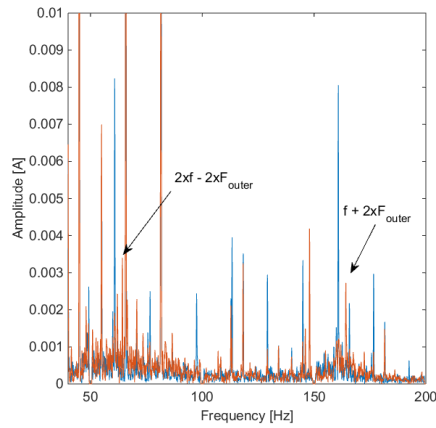


Figure 6: Comparison of FFT spectra of the notch-filtered current signal of the MUT operated at rated output torque and 6 bar pressure on the radial load cylinder: healthy bearing (blue), faulty bearing with localized outer race defect (red).

In a deep groove ball bearing the impact forces due to the bearing fault act along a radial direction mainly. It is reasonable to expect the torque ripple related to the bearing fault to be dependent upon radial load, but to be independent of the torque transmitted by the shaft. From preliminary observations on the radial vibration signals, no significant difference was observed between the test run with the MUT operating at no torsional load and at rated-torque: if the fault is present, fault signature is evident regardless of output torque.

There are a number of approaches to represent the results graphically to demonstrate the effects of the variables on the system outputs. One of the most popular is the normal plot, used to estimate whether a certain set of data follows a Gaussian distribution or not. If the data approximates a straight line the phenomenon is statistically "normal" i.e. follows a stochastic law. The variables affecting the system response will then fall outside the normal distribution line, thus their effect cannot be ascribed to a stochastic process. The greater the deviation of the point from the normal line the larger the confidence interval (i.e. the probability that the variables are significant is higher). The half normal plot, used in this paper is interpreted in the same way as the normal plot but allows absolute values of the effects to be considered. Figure 7 shows the half-normal probability plots from an analysis of the variance (ANOVA) test of current signals fault indicator in case of single point defect (on the left) and brinelling defect (on the right).

The ANOVA highlights the effects that significantly influence a physical phenomenon by comparing these effects of the output variable with a stochastic effect. This is obtained by comparing the results coming from the several levels of the selected experimental variable, driven by the stochastic experimental error. These values represent the probability that the effect of the variable is significant.

Half normal plots show the magnitude of the experiment's effects ordered in increasing magnitude along the x-axis. The effect for a factor is the difference of the average response variable over "high" factor levels minus the average response over the "low" factor levels. As said before, half normal plot show the distribution of the $\text{abs}(X)$ with X having a normal distribution with mean zero. The points comprising factors with small and/or insignificant effects on the response will describe (roughly) a straight line on the plot. The points for factors with a 'large' and thus significant effects will visually fall off of the straight line described by the insignificant factors. A line through the insignificant factors helps to graphically delineate the difference between significant and insignificant factors. To visually interpret half normal plots: selecting the factor points which lie reasonably off of the line describing insignificant factors is an easy graphical way to identify important factors and start the process of optimizing the model. Further details and additional statistical information on the half normal plot construction can be found in [18] and [19].

Concerning the first test set on a single point defect on the outer race, the left part of Fig. 7 shows the half normal plot of the current fault indicator: as it can be seen, only the effect of the fault presence is significant, while load torque and radial load and their interactions have negligible effect.

Concerning the second test set on a simulated brinelling fault the right part of Fig. 7 shows the half normal plot of the current fault indicator: as it can be seen, only the effect of the fault presence is significant, while load torque and radial load and their interactions have negligible effect.

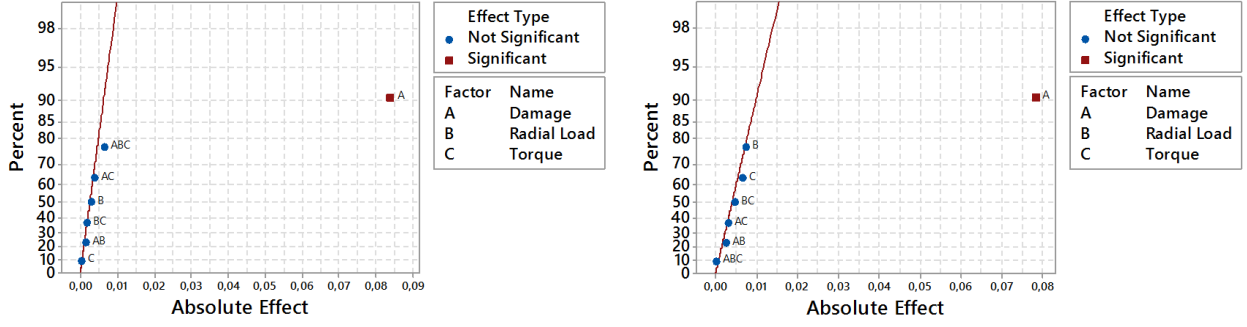


Figure 7: Test set 1 (single point defect on outer race): Half normal plot of the scalar current fault indicator (left). Test set 2 (brinelling defect): Half normal plot of the scalar current fault indicator (right).

It is worth pointing out that with the present test setup, the maximum pressure in the pneumatic cylinder (6 bar) results in a radial loading force that is 1/6 of the maximum permissible static force provided by the bearing’s manufacturer. This represents a normal working condition: much higher values of load could cause an increase of the importance of radial load factor, but would result in reduced lifetime of the bearing and not typical of practical applications in everyday use.

5.2 LSTM results

The deep network used in the fault detection experiments is composed of two LSTM layers, each of them containing 100 cells, followed by other two dense layers containing 100 neurons each (this is a classical feed-forward neural network), followed by one output neuron. A dropout value $p = 0.5$ and a batch size equal to 64 were used for training. The network was trained with the RMSprop algorithm, using an initial learning rate $\eta = 5 \cdot 10^{-5}$. Concerning the data input, a window $W = 300$ was used and, as customary with neural networks, all the features were normalized in the $[0, 1]$ interval using the statistics computed on the training set.

The data analysis task began with the simple binary classification of distinguishing faulty cases (class F) from normal healthy operation (class H). To obtain the training set, data coming from the experiment with 50% radial load and 50% output torque was used, the data set related to experiments with a single defect on the outer raceway represented the faulty class. To construct the validation set, the same cases were employed, but pertaining to experiments with the radial load level equal to 100%. A relevant point is that no datasets related to the brinelling fault experiments were used for training nor for validation sets.

In order to evaluate the proposed approach, we employ standard metrics in machine learning, such as accuracy, precision, recall, and F_1 . When dealing with a binary classification task True Positives (TP) and True Negatives (TN) are respectively the number of examples of the positive/negative class that are correctly classified. False Positives (FP) are the negative (healthy) examples that are mistakenly classified as positives, the opposite cases are False Negatives (FN). Accuracy A is defined as the total percentage of correct predictions:

$$A = \frac{TP + TN}{TP + TN + FP + FN} \quad (6)$$

Precision P and recall R are related to the ratio of false positives and false negatives:

$$P = \frac{TP}{TP + FP} \quad (7)$$

and

$$R = \frac{TP}{TP + FN} \quad (8)$$

Finally F_1 is the harmonic mean between P and R ,

$$F_1 = \frac{2PR}{P + R} \quad (9)$$

In our first experiment, the test set is the setting with half radial load, and maximum output torque: in this case we achieve $A = 0.759$, $P = 0.924$, $R = 0.564$, $F_1 = 0.700$, so that the network detects over than half of the faulty examples, with less than 8% of false positives (see confusion matrix in Table 5, left). If we apply a post-processing filter, where we detect a sample as faulty if at least m of the past n samples were predicted as faulty, then performance rapidly improves. The parameters m and n can be chosen so as to balance the number of FP and FN. For example, keeping $n = 1,000$ we achieve $P = 0.840$ and $R = 0.990$ with $m = 100$, whereas we obtain $P = 0.940$ and $R = 0.960$ with $m = 200$. In the former setting, almost all the faults are detected, but the number of FP raises to 16% while in the latter the two types of errors are more balanced.

In our second set of experiments, we considered the network trained in the first setting, and we evaluate its performance with several different test sets. In absence of radial load, we achieve $P = 0.849$ and $R = 0.818$ with full output torque, and $P = 0.931$ and $R = 0.594$ with half output torque (see confusion matrices in Table 5, center and right, respectively). The brinnelling fault is almost perfectly detected as well, with an accuracy equal to 0.984 and 0.998 with half and full output torque, respectively (radial load is kept fixed at 50%).

This result confirms that the datasets obtained with experiments at different radial loads can be used both for training and for validation, to avoid overfitting of the LSTM.

%	H	F	%	H	F	%	H	F
H	47.68	2.33	H	47.80	2.21	H	42.74	7.26
F	21.79	28.20	F	20.31	29.68	F	9.09	40.91

Table 5: Confusion matrices for three different test sets. Left: 50% radial load, 100% output torque; center: no radial load, 50% output torque; right: no radial load, 100% output torque. Rows: true labels, columns: predicted values.

6 Conclusions

This paper details the results of a laboratory trial comprising different test sets on the condition monitoring and fault diagnostic of a six-poles induction motor, using a design of experiment (DOE) approach. The DOE allows some considerations about the influence of external radial loads applied to the output shaft of the motor. A scalar fault indicator based on current signal has been proposed as fault detector. This indicator proved to positively identify the faulted case versus the healthy one. The main results of the DOE are that output torque, radial load and their interactions have negligible effect on scalar fault indicators. Only the effect of the fault presence is significant. This indicates a fair robustness of the chosen scalar fault indicators under different operating conditions and in case of different faults. Finally, the radial load has no relevant effect on the current signals in case of healthy bearing. The occurrence of false positive fault detection due to radial load is avoided. The same scalar fault indicator based on current signal has been taken as input to a Long Short-Term Memory network to test a machine learning approach for the fault detection of the bearings. The main results are that the proposed LSTM fault detection positively identify the fault case with respect to the healthy one. It can be efficiently trained on an easily reproducible single defect case, and then be employed to identify a more complex fault. Finally, the proposed LSTM fault detection showed a fair robustness of detection under different operating conditions and in case of different faults.

Acknowledgements

The authors are grateful for the National University Research Fund (FAR 2018) of the University of Modena and Reggio Emilia - Departmental and Interdisciplinary Projects - DEep LEarning Condition moniToring (DEfLECT).

References

- [1] S. Nandi, H. A. Toliyat, and X. Li, “Condition monitoring and fault diagnosis of electrical motors-a review,” *IEEE Transactions on Energy Conversion*, vol. 20, no. 4, pp. 719–729, Dec 2005.

- [2] A. Garcia-Perez, R. d. J. Romero-Troncoso, E. Cabal-Yepez, and R. A. Osornio-Rios, "The application of high-resolution spectral analysis for identifying multiple combined faults in induction motors," *IEEE Transactions on Industrial Electronics*, vol. 58, no. 5, pp. 2002–2010, May 2011.
- [3] A. H. Bonnett, "Root cause ac motor failure analysis with a focus on shaft failures," *IEEE Transactions on Industry Applications*, vol. 36, no. 5, pp. 1435–1448, Sep 2000.
- [4] C. Bianchini, F. Immovilli, M. Cocconcelli, R. Rubini, and A. Bellini, "Fault detection of linear bearings in brushless ac linear motors by vibration analysis," *IEEE Transactions on Industrial Electronics*, vol. 58, no. 5, pp. 1684–1694, May 2011.
- [5] F. Immovilli, G. Curcurú, M. Cocconcelli and R. Rubini, "On the detection of distributed roughness on ball bearings via stator current energy: Experimental results," *Diagnostyka*, vol. 51, no. 3, pp. 17–21, 2009.
- [6] R. Rubini and U. Meneghetti, "Application of the envelope and wavelet transform analysis for the diagnosis of incipient faults in ball bearings," *Mechanical Systems and Signal Processing*, vol. 15, no. 2, pp. 287 – 302, 2001.
- [7] J. R. Stack, T. G. Habetler, and R. G. Harley, "Fault-signature modeling and detection of inner-race bearing faults," *IEEE Transactions on Industry Applications*, vol. 42, no. 1, pp. 61–68, Jan 2006.
- [8] M. Blodt, M. Chabert, J. Regnier, and J. Faucher, "Mechanical load fault detection in induction motors by stator current time-frequency analysis," *IEEE Transactions on Industry Applications*, vol. 42, no. 6, pp. 1454–1463, Nov 2006.
- [9] F. Immovilli, C. Bianchini, M. Cocconcelli, A. Bellini, and R. Rubini, "Bearing fault model for induction motor with externally induced vibration," *IEEE Transactions on Industrial Electronics*, vol. 60, no. 8, pp. 3408–3418, Aug 2013.
- [10] S. Choi, B. Akin, M. M. Rahimian, and H. A. Toliyat, "Performance-oriented electric motors diagnostics in modern energy conversion systems," *IEEE Transactions on Industrial Electronics*, vol. 59, no. 2, pp. 1266–1277, Feb 2012.
- [11] S. Hochreiter, and J. Schmidhuber, "Deep learning," *Neural computation*, vol. 9, no. 8, pp. 1735-1780, 1997.
- [12] R. A. Fisher, *The design of experiments*. Hafner Publishing Company, 1971.
- [13] M. Blodt, D. Bonacci, J. Regnier, M. Chabert, and J. Faucher, "On-line monitoring of mechanical faults in variable-speed induction motor drives using the wigner distribution," *IEEE Transactions on Industrial Electronics*, vol. 55, no. 2, pp. 522–533, Feb 2008.
- [14] C. M. Riley, B. K. Lin, T. G. Habetler, and R. R. Schoen, "A method for sensorless on-line vibration monitoring of induction machines," *IEEE Transactions on Industry Applications*, vol. 34, no. 6, pp. 1240–1245, Nov 1998.
- [15] M. Blodt, P. Granjon, B. Raison, and G. Rostaing, "Models for bearing damage detection in induction motors using stator current monitoring," *IEEE Transactions on Industrial Electronics*, vol. 55, no. 4, pp. 1813–1822, April 2008.
- [16] F. Immovilli, A. Bellini, R. Rubini, and C. Tassoni, "Diagnosis of bearing faults in induction machines by vibration or current signals: A critical comparison," *IEEE Transactions on Industry Applications*, vol. 46, no. 4, pp. 1350–1359, July 2010.
- [17] D. C. Montgomery, *Design and Analysis of Experiments*. Wiley and sons, 2012.
- [18] D. Cuthbert, "Use of half-normal plots in interpreting factorial two-level experiments", *Technometrics*, vol. 1, no. 4, pp. 311 – 341, 1959.

- [19] M. J. Anderson and P. J. Whitcomb, *DOE Simplified: Practical Tools for Effective Experimentation, Second Edition*. Productivity Press, 2007.
- [20] K. Greff, R. K. Srivastava, J. Koutník, B. R. Steunebrink, and J. Schmidhuber, “LSTM: A Search Space Odyssey”, *IEEE Transactions on Neural Networks and Learning Systems*, vol. 99, pp. 1 – 11, 2017.
- [21] Y. Bengio, P. Simard, and P. Frasconi, “Learning long-term dependencies with gradient descent is difficult”, *Neural Networks, IEEE Transactions on*, vol. 5, no. 2, pp. 157 – 166, 1994.
- [22] N.. Srivastava, G.. Hinton, A. Krizhevsky, I. Sutskever, and R. Salakhutdinov, “Dropout: A simple way to prevent neural networks from overfitting”, *Journ. Mach. Learn. Res.*, vol. 15, no. 1, pp. 1929 – 1958, 2014.